

Cantilever magnetometry of individual Ni nanotubes

D. P. Weber, D. Ruffer, A. Buchter, F. Xue, E. Russo-Averchi, R. Huber, P. Berberich, A. Fontcuberta i Morral, D. Grundler, and M. Poggio.

Full Derivation of Model

In order to interpret our data we begin by making the simplifying assumption that our nanotube behaves as a single-domain magnetic particle, i.e. its magnetization is uniform and rotates in unison. For high enough applied fields, the nanotube is magnetized to saturation, and thus this single-domain assumption is valid. We therefore describe the nanotube's magnetic state by the orientation of its total magnetization vector \mathbf{M} . More complex states deviating from this assumption will be addressed separately later. Since the Ni nanotube is polycrystalline and does not exhibit magneto-crystalline anisotropy, we assume the nanotube to exhibit only shape anisotropy. The total energy of the system can be written as the sum of the cantilever energy, the Zeeman energy, and an effective anisotropy energy:

$$E = \frac{1}{2}k_0(l_e\theta)^2 - MVH \cos(\theta - \phi) + KV \sin^2 \phi, \quad (\text{S1})$$

where V is the volume of the nanotube, K is its anisotropy in the plane of the cantilever oscillation and ϕ is the angle between \mathbf{M} and \hat{z}' . In order to calculate ϕ , we minimize the energy of the system with respect to this angle. The solutions must satisfy both $\partial E/\partial \phi = 0$ and $\partial^2 E/\partial \phi^2 > 0$, giving:

$$HM \sin(\theta - \phi) = 2K \cos \phi \sin \phi, \quad (\text{S2})$$

$$HM \cos(\theta - \phi) + 2K(\cos^2 \phi - \sin^2 \phi) > 0. \quad (\text{S3})$$

Solutions for ϕ are difficult to obtain exactly, however, since $\theta \ll 1$, we can expand ϕ as a function of θ to first order around $\theta = 0$:

$$\phi(\theta) = \phi_0 + \left(\frac{\partial \phi}{\partial \theta}\right)_0 \theta. \quad (\text{S4})$$

Returning to (S2) we find for $\theta \ll 1$:

$$\theta = \frac{2K}{HM} \sin \phi + \tan \phi. \quad (\text{S5})$$

Solving for ϕ_0 at $\theta = 0$ and using $\left(\frac{\partial \phi}{\partial \theta}\right)_0 = 1/\left(\frac{\partial \theta}{\partial \phi}\right)_{\phi=\phi_0}$ we find solutions in the form of (S4).

Applying (S3) for ϕ_0 and $\theta = 0$, we find limits on the stability of each solution,

$$\phi = \begin{cases} \left(\frac{H}{H+\frac{2K}{M}}\right)\theta & \text{for } H > -\frac{2K}{M} \\ \pi + \left(\frac{H}{H-\frac{2K}{M}}\right)\theta & \text{for } H < \frac{2K}{M} \\ \pm \arccos\left(-\frac{MH}{2K}\right) + \left(\frac{H^2}{\left(\frac{2K}{M}\right)^2 - H^2}\right)\theta & \text{for } K < 0 \text{ and } |H| < \left|\frac{2K}{M}\right| \end{cases} \quad (\text{S6})$$

We then substitute the expansion (S4) for $\phi(\theta)$ into the expression for the torque acting on the cantilever, $\tau = -\partial E/\partial\theta = -k_0 l_e^2 \theta - HMV \sin(\theta - \phi)$. Using (S2) and keeping only terms up to first order in θ , we find,

$$\tau = -KV \sin(2\phi_0) - \left[k_0 l_e^2 + 2KV \cos(2\phi_0) \left(\frac{\partial\phi}{\partial\theta}\right)_0 \right] \theta. \quad (\text{S7})$$

The left-most term in (S7) produces a constant deflection of the cantilever, while the term proportional to θ determines the cantilever's spring constant. Approximating the cantilever as a simple harmonic oscillator, we have:

$$m_e \ddot{x} + \Gamma \dot{x} = \frac{\tau}{l_e}, \quad (\text{S8})$$

where m_e is the effective mass of the cantilever and Γ is the cantilever's dissipation. Therefore,

$$m_e \ddot{x} + \Gamma \dot{x} + \left[k_0 + \frac{2KV}{l_e^2} \cos(2\phi_0) \left(\frac{\partial\phi}{\partial\theta}\right)_0 \right] x = -\frac{KV}{l_e} \sin(2\phi_0). \quad (\text{S9})$$

Solving this equation of motion we find the angular resonance frequency of the cantilever:

$$\omega = \sqrt{\frac{k_0}{m_e} + \frac{2KV}{m_e l_e^2} \cos(2\phi_0) \left(\frac{\partial\phi}{\partial\theta}\right)_0 - \frac{\Gamma^2}{4m_e^2}}. \quad (\text{S10})$$

We define $\omega_0 = \sqrt{\frac{k_0}{m_e}}$ and solve for the angular frequency shift $\Delta\omega = \omega - \omega_0$:

$$\Delta\omega = \omega_0 \left(\sqrt{1 + \frac{2KV}{m_e \omega_0^2 l_e^2} \cos(2\phi_0) \left(\frac{\partial\phi}{\partial\theta}\right)_0 - \frac{\Gamma^2}{4m_e^2 \omega_0^2}} - 1 \right). \quad (\text{S11})$$

Since the last two terms in the square-root are small compared to 1, we expand (S11) to first order in these small parameters:

$$\Delta\omega = \frac{\omega_0}{2k_0} \left[\frac{2KV}{l_e^2} \cos(2\phi_0) \left(\frac{\partial\phi}{\partial\theta}\right)_0 - \frac{\Gamma^2}{4m_e} \right]. \quad (\text{S12})$$

In practice, the cantilevers used in these experiments show a small enough dissipation that the last term in (S12) is negligible, resulting in:

$$\Delta\omega = \frac{\omega_0}{2k_0 l_e^2} \left[2KV \cos(2\phi_0) \left(\frac{\partial\phi}{\partial\theta}\right)_0 \right]. \quad (\text{S13})$$

Combining (S6), (S13), and $\Delta f = \Delta\omega/(2\pi)$, we calculate the expected frequency shifts as a function of H :

$$\Delta f = \begin{cases} \frac{\omega_0}{4\pi k_0 l_e^2} \left(\frac{2HKV}{H + \frac{2K}{M}} \right) & \text{for } H > -\frac{2K}{M} \\ \frac{\omega_0}{4\pi k_0 l_e^2} \left(\frac{2HKV}{H - \frac{2K}{M}} \right) & \text{for } H < \frac{2K}{M} \\ \frac{\omega_0}{4\pi k_0 l_e^2} \left[\frac{H^2 M^2 V}{2K} \left(\frac{2H^2 - \left(\frac{2K}{M}\right)^2}{\left(\frac{2K}{M}\right)^2 - H^2} \right) \right] & \text{for } K < 0 \text{ and } |H| < \left| \frac{2K}{M} \right| \end{cases} . \quad (\text{S14})$$

Singularities at $H = \pm \frac{2K}{M}$ reflect the break-down of the small angle approximation and the solutions become invalid near this field. The first two solutions correspond to \mathbf{M} pointing along $\pm \hat{z}$ respectively. The third solution, valid only for $K < 0$, corresponds to \mathbf{M} along an easy axis perpendicular to \hat{z} (the implication of a negative K) and rotating toward \hat{z} with increasing H .

Fabrication



Fig. S1: Motion picture of the sample fabrication, from optical micrographs. Two main steps are involved in the process, first, glueing of the cantilever tip, and second, attachment of the Ni nanotube. In preparation, a glass rod has been pulled to form a sharp tip and inserted into a micromanipulator setup.

Samples

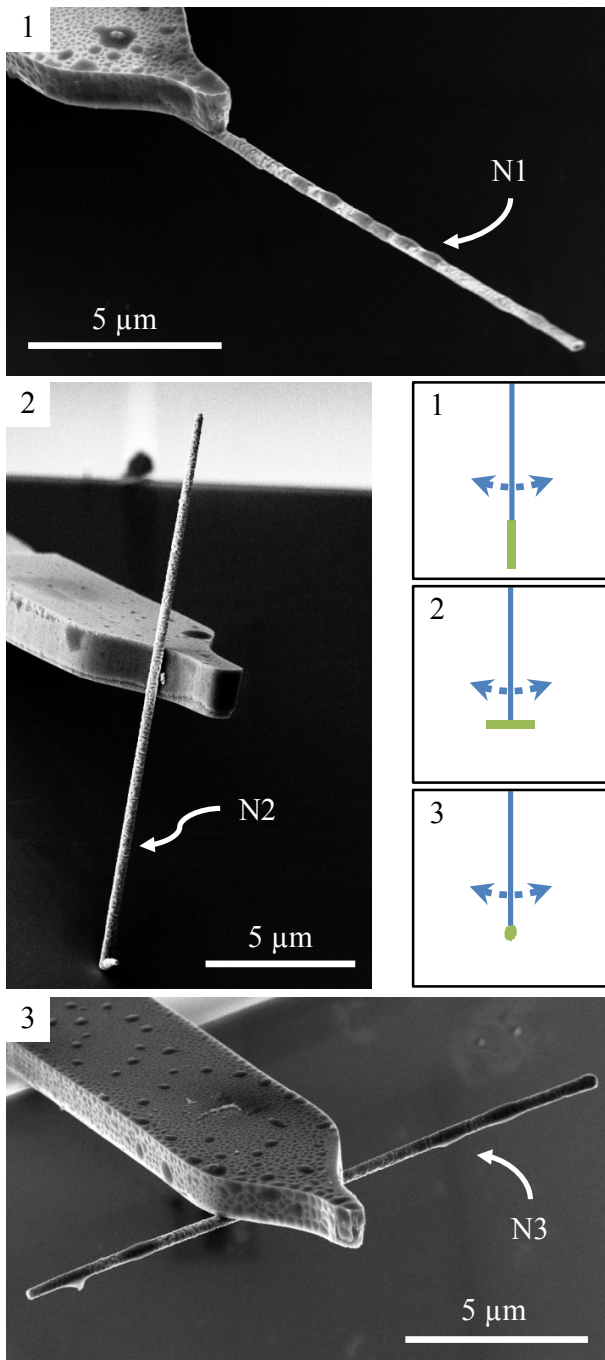


Fig. S2: Scanning electron microscopy (SEM) images showing the three configurations of the Ni nanotubes N1, N2, and N3. Each nanotube is affixed to the end of an ultrasensitive Si cantilever. The liquid-like material visible on the cantilevers is likely due to hydrocarbon adsorption during the long periods in the cryogenic measurement system. This material is non-magnetic and has not been seen to affect the magnetic response of our measurements. Three schematic diagrams (1, 2, and 3) show the corresponding plane of the cantilevers oscillation, with the nanotube's symmetry axis aligned along \hat{z} , \hat{x} , and \hat{y} , respectively (see also main article, Fig. 1).

Step-like Structures in Configuration 1

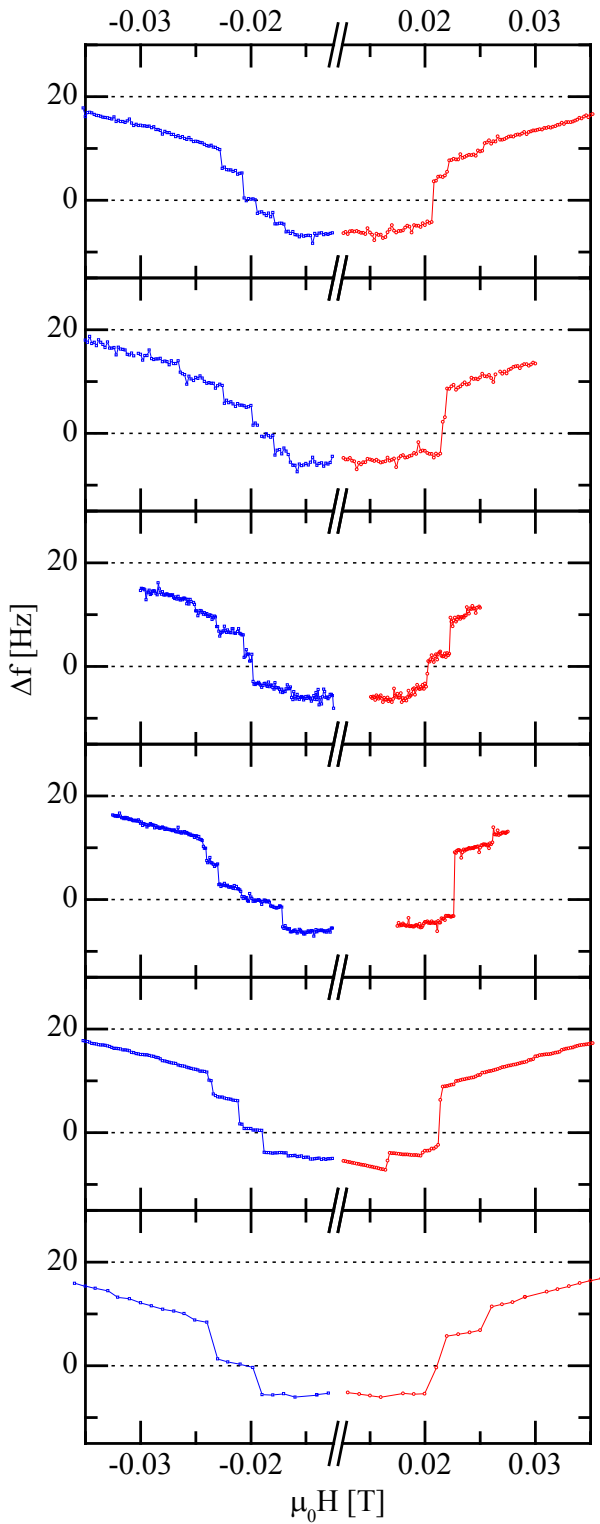
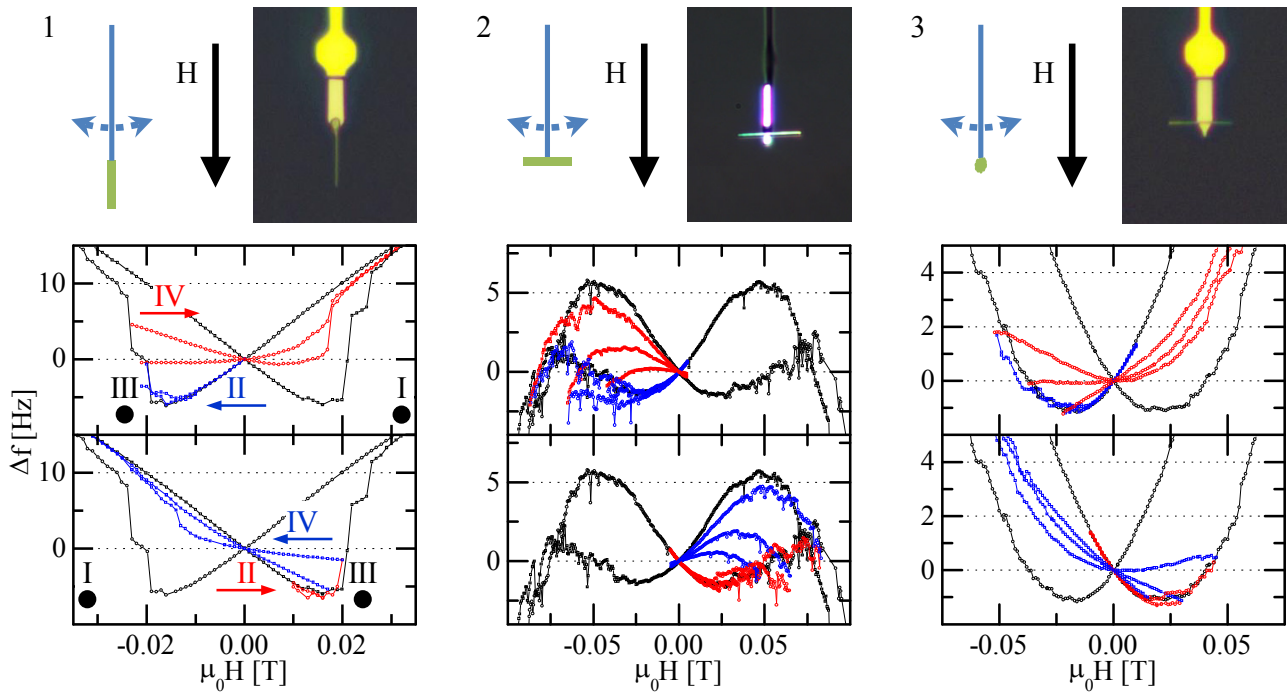


Fig. S3: Cantilever magnetometry measurements in configuration 1 (the nanotube's symmetry axis is aligned along \hat{z}). Red (blue) points represent data taken while sweeping H in the positive (negative) direction. Averaging times and step sizes taken vary with each measurement.

At low fields between 150 and 250 mT the data show step-like structures, the field positions of the steps vary slightly with each measurement. These steps cannot be described by a uniform magnetization model. The presence of discrete steps indicates three to four multi domain states (MDSs), intermediate between two uniform axial states (UASs). Behavior asymmetric with respect to the sweep direction may be due to actual geometrical asymmetries of the Ni nanotube. Steps around $\Delta f = 0$ (for non-zero fields) may suggest a preference for a global vortex state (GVS).

Minor Hysteresis Loops



Sample Specifications

Configuration	Si Cantilever					Nanotube	Ni Nanotube				
	Length [μm]	Effective Length l_e [μm]	Resonant Frequency f_0 [Hz]	Spring Constant k_0 [$\mu\text{N/m}$]	Q-Factor Q_0		Length l [μm]	Outer Diameter [†] [nm]		Ni Shell Thickness t [nm]	Volume V [μm^3]
								max. D_o	min. d_o		
1	150	105.4	2808.5 (2801.9) [*]	70 \pm 10	25000	N1	21.0 \pm 0.5	360 \pm 8	303 \pm 5	44 \pm 9	0.83 \pm 0.18
2	150	105.4	2093.8 [†]	50 \pm 10	42000	N2	19.8 \pm 0.5	381 \pm 6	270 \pm 4	44 \pm 9	0.77 \pm 0.16
3	150	105.4	2782.6 (2781.0)	50 \pm 15	22000 (15000)	N3	18.2 \pm 0.5	349 \pm 5	274 \pm 5	44 \pm 9	0.67 \pm 0.14

Table S1: Properties of the Si cantilever and Ni nanotube sample for each configuration. ^{*}Numbers in parentheses reflect the change in mass of the cantilever after one cool-down/warm-up cycle, likely due to adsorption of hydrocarbons or water present in the air. [†]Here the frequency is significantly lower compared to the other cantilevers of the same type. This frequency shift can be explained by an additional drop of glue unintentionally put on the cantilever. ^{*}The volume of the nanotube is calculated as a shallow, truncated cone:

$$V = \pi l t \left(\frac{D_o + d_o}{2} - t \right)$$